

Fig. 5. Schematic diagram of the comprehensive Bailey [15] model for quartz.

explanation of the levels, the reader is referred to Bailey [15]:

- Level 1 represents the 110 °C TL shallow electron trap, which gives rise to a TL peak at ~ 100 °C when measured with a heating rate of 5 K s^{-1} ,
- level 2 represents a generic 230 °C TL level, as found in many sedimentary quartz samples. Photo-excitation of charge from this level is not allowed,
- levels 3 and 4 are usually termed ‘fast’ and ‘medium’ OSL components (e.g., [33]) and yield TL peaks at ~ 330 °C as well as give rise to the OSL emission used for dating,
- level 5 is a deep, thermally disconnected electron trap. This was proposed in order to explain several TL and OSL phenomena based on competition between energy levels,
- levels 6–9 are hole trapping centres acting as recombination centres for optically or thermally released electrons or for electrons which recombine directly after they reached the conduction band. Levels 6 and 7 are defined as thermally unstable, non-radiative recombination centres, similar to the hole reservoirs first introduced by Zimmerman [34,16] in order to explain the pre-dose sensitization phenomenon in quartz. Level 8 is a thermally stable, radiative recombination centre termed the ‘luminescence’ (L) centre. Level 9 is defined as a thermally stable, non-radiative recombination centre termed ‘killer’ (K) centre. Holes can be thermally transferred from the two hole reservoirs (levels 6 and 7, R_1 and R_2) into the luminescence centre and the killer centre via the valence band.

Pagonis et al. [35] stated that the levels 1, 6, 7 and 8 play a fundamental role for the pre-dose phenomenon, while we will argue in Section 4.3 that levels 5, 6 and 8 are vital for reproducing the UV-RF experimental results shown in Section 3 with the chosen model of Bailey [15].

The following differential Eqs. (1)–(4) describe the charge flow in quartz in the context of luminescence production and are to be solved in this study. The total number of equations that need to be solved depends on the number of electron traps (q) and hole centres (r). For the case of the complete Bailey [15] model $q=5$ and $r=4$. In Section 4.3 we use a simplified model with $q=1$ and $r=2$.

$$\frac{dn_i}{dt} = n_c \cdot (N_i - n_i) \cdot A_i - n_i \cdot P \cdot \sigma_{0i} \cdot e^{-E_{thi}/(k_B T)} - n_i \cdot S_i \cdot e^{-E_{ji}/(k_B T)} \quad (1)$$

$$\frac{dn_j}{dt} = n_v \cdot (N_j - n_j) \cdot A_j - n_j \cdot S_j \cdot e^{-E_{jl}/(k_B T)} - n_c \cdot n_j \cdot B_j \quad (2)$$

$$\frac{dn_c}{dt} = R - \sum_{i=1}^q \left(\frac{dn_i}{dt} \right) - \sum_{j=q+1}^{q+r} (n_c \cdot n_j \cdot B_j) \quad (3)$$

Table 1

Description of the abbreviations used in the differential equations.

Abbreviation	Description	Unit
n_c	Concentration of electrons in the conduction band	cm^{-3}
n_v	Concentration of holes in the valence band	cm^{-3}
N_i	Concentration of electron traps	cm^{-3}
n_i	Concentration of trapped electrons	cm^{-3}
S_i	Frequency factor for electron traps	s^{-1}
E_i	Electron trap depth below the conduction band	eV
N_j	Concentration of hole centres	cm^{-3}
n_j	Concentration of trapped holes in centres	cm^{-3}
S_j	Frequency factor for hole centres	s^{-1}
E_j	Hole depth above the valence band	eV
A_i	Conduction band to electron trap transition probability	$\text{cm}^3 \text{ s}^{-1}$
A_j	Valence band to hole centre transition probability	$\text{cm}^3 \text{ s}^{-1}$
B_j	Conduction band to hole centre transition probability	$\text{cm}^3 \text{ s}^{-1}$
P	Stimulation photon flux	
σ_{0i}	Photo eviction constant	s^{-1}
E_{thi}	Thermal assistance energy	eV
k_B	Boltzmann constant	eV K^{-1}
T	Absolute temperature	K
R	Ionisation rate (pair production rate)	$\text{cm}^{-3} \text{ s}^{-1}$
t	Time	s

$$\frac{dn_v}{dt} = R - \sum_{j=q+1}^{q+r} \left(\frac{dn_j}{dt} \right) - \sum_{j=q+1}^{q+r} (n_c \cdot n_j \cdot B_j) \quad (4)$$

A short description of the used abbreviations is given in Table 1 and in detail in Bailey [15].

Table 3 shows in schematic form the steps simulated for the experiments shown in Section 2. After each excitation stage in the simulations a relaxation period is introduced in which the temperature of the sample is kept constant at 20 °C for 60 s after the excitation has stopped ($R=0$), and the concentrations of n_c and n_v decay to negligible values. When the temperature of the next simulation step is not the same as in the current step, the numerical solution simulates a cooling or heating period with a constant rate of $\beta=5 \text{ K s}^{-1}$.

Bailey [15] originally administered the burial dose at an elevated temperature of 220 °C and used a very high dose rate of 0.01 Gy s^{-1} (step 7 in Table 3). In the modified step 7 above, we used a much lower dose rate of $10^{-11} \text{ Gy s}^{-1}$ for the burial dose. This dose rate is closer to the typical environmental dose rate values, and an irradiation temperature of 20 °C [36]. Step 1 in Table 3 is simulated with a dose rate of 1 Gy s^{-1} in order to reduce computation times. Step 3 (‘geological time’) is used to empty shallow electron traps and hole centres. Thus, thermally unstable traps and centres are minimally populated after step 3. These conditions are supported by measurements of natural quartz samples (for details see [15], Section 2.5).

It is well known for quartz that thermal transfer can take place from the hole reservoirs (level 6 and 7 in Table 2) into the L-centre (level 8 in Table 2), causing sensitivity changes in general and specifically the pre-dose effect [16,34].

As discussed in Bailey [15], the ionization rate R depends on the exact experimental conditions, namely the strength of the irradiation source and the irradiation geometry. The choice of the R value in the Bailey [15] model is arbitrary; hence we adjusted this value so that the simulated RF results are similar to our experimental RF data.

For the simulations shown here we used the same ionization rate as Bailey [15], except for step 10 of the simulation sequence (Table 3), where we employed a dose rate of 0.006 Gy s^{-1} , which

Table 2

The Qtz-A₁ parameters of [15] are shown together with their modified values used in the simulations presented in this study (bold values).

	Levels	N [cm ⁻³]	E [eV]	s [s ⁻¹]	A [cm ³ s ⁻¹]	B [cm ³ s ⁻¹]	σ_0 [s ⁻¹]	E_{th} [eV]
1	110 °C TL	1.5e7	0.97	5e12	1e-8	–	0.75	0.1
2	230 °C TL	1e7	1.55	5e14	1e-8	–	–	–
3	OSL _F	1e9	1.7	5e13	1e-9	–	6	0.1
4	OSL _M	2.5e8	1.72	5e14	5e-10	–	4.5	0.13
5	Deep	5e10	2	1e10	1e-10	–	–	–
6	R ₁ -centre	3e8	3e9	5e13	5e-7	5e-9	–	–
7	R ₂ -centre	1e10	1.75	5e14	1e-9	5e-10	–	–
8	L-centre	1e11	5	1e13	1e-9	1e-10	–	–
9	K-centre	5e9	5	1e13	1e-10	1e-10	–	–

Table 3

The simulation steps for the UV-RF simulation. For each new preheat temperature a new (simulated) aliquot was used. Steps 9 and 10 represent the simulated measurements in the laboratory.

1	Geological dose irradiation of 1000 Gy at 1 Gy s ⁻¹ at 20 °C
2	Relaxation stage - 60 s at 20 °C
3	Geological time - heat from 20 °C to 350 °C at 5 °C s ⁻¹
4	Relaxation for geological time, 60 s at 20 °C
5	Illuminate for 100 s at 200 °C - repeated daylight exposures over long time
6	Relaxation stage - 60 s at 20 °C
7	Burial dose - 50 Gy at 20 °C at 10 ⁻¹¹ Gy s ⁻¹
8	Relaxation stage - 60 s at 20 °C
9	Preheat to temperatures from 50 °C to 500 °C (in 50 °C increments) for 120 s
10	Radiofluorescence for 10,000 s at 20 °C at 0.006 Gy s ⁻¹

is an order of magnitude smaller than the experimental dose rate. With such a dose rate, we obtained good accordance between UV-RF experiments and simulations, so that our modelling approach for the first time quantitatively reproduces UV-RF of natural quartz samples.

4.2. Matching experimental results and simulations

Fig. 6 shows the result of the RF simulations for different preheat treatments (see Table 3, step 9). The signals decrease over the observation time, but, as in the experimental data, for low temperatures signal dynamics are very weak. At a preheat temperature of 300 °C a change in the decay curve shape is observable. For preheat temperatures from 550–700 °C the signal intensity

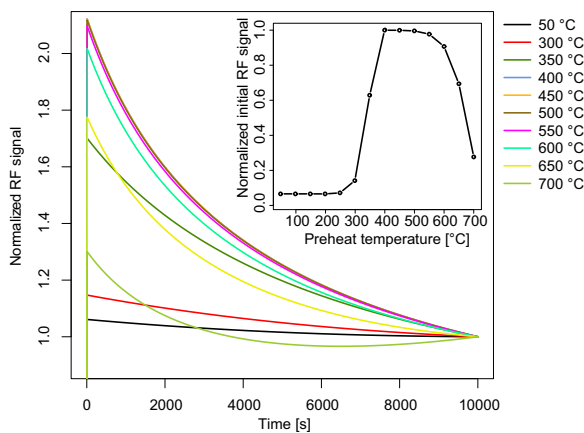


Fig. 6. Simulation of the sequence presented in Table 3 with the parameters from Table 2. The RF signal is normalized to the last signal value at 10,000 s. The inset shows the simulated initial RF signal from the main figure. The values on the y-axis are normalized to the highest value of all initial signals.

decreases again.

Besides the signal intensity, the most striking observation is the change in the decaying UV-RF signal. This effect can be related to a changing proportion of holes in the R-centres and L-centre. With higher preheat temperatures the concentration in the L-centre increases, see Fig. 9. The decay of the UV-RF signal can be linked to an increasing competition between the R-/K-centres and the L-centre during irradiation. This observation and a detailed explanation of this effect will be presented elsewhere.

This seems to qualitatively reproduce the experimental results from Figs. 1 and 2: The inset of Fig. 6 shows that the simulated initial RF signal does not change for low temperatures and at temperatures about 300 °C a massive increase of the signal occurs until a maximum value is reached at 400 °C. The higher the preheat temperatures are from now on the smaller is the initial signal intensity. Thus this simulation enables to reproduce qualitatively the signal dynamics and the signal height of the measured RF signal. However, the accordance is not quantitatively perfect for both natural samples.

To quantitatively simulate experimental RF signals, a more accurate determination of the model parameters (Table 2) is necessary, which is, however, not part of this study. Nevertheless, the behaviour of sample BT586 for a preheat temperature of 700 °C was not reproducible by our numerical simulations.

The second set of experiments was the successive preheat and RF measurement for 11 cycles, see Fig. 4. The simulation for this sequence is shown in Fig. 7 and, as in the experiments with natural samples, a continuous growth of the initial signal intensity was observed from cycle to cycle. Note that before the first UV-RF measurement a preheat to 500 °C was performed. Otherwise, the

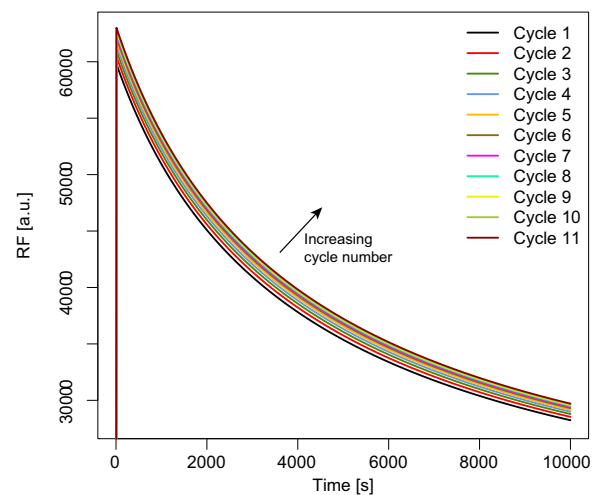


Fig. 7. Simulation of the experimental results from Fig. 4. Following the sample history, a preheat to 500 °C and a subsequent RF step were simulated, see steps 9 and 10 in Table 3.

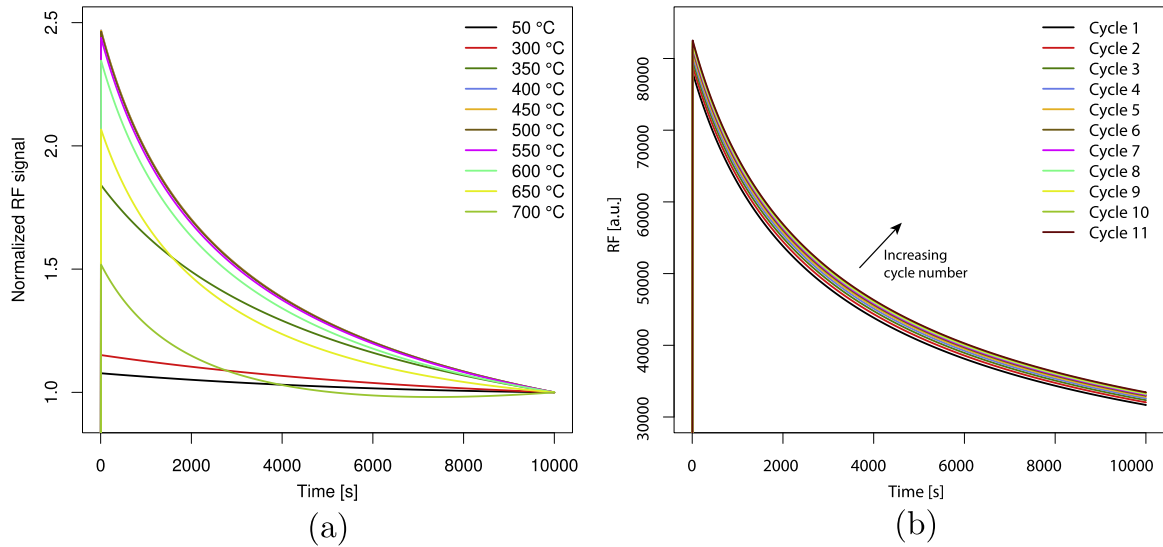


Fig. 8. (a) Same simulation as for Figs. 6 and 7 (b) but using the simplified model with energy levels 5, 6 and 8 only (see Table 2).

signal for the first cycle would not decrease over time. In contrast to the experimental data, the signal for cycle 1 has the same curvature as all other cycles and so only the signal height is changing for each new cycle.

4.3. Further simulation results

In order to understand the charge movements of the UV-RF signal with different preheat temperatures, we simplified the used quartz model down to three energy levels, which produces approximately the same results as the complete model, but is easier to interpret.

For this purpose the deep electron trap, the R₁-centre and the L-centre were chosen. Figs. 8(a) and (b) show the same simulations as Figs. 6 and 7 but with only three energy levels and the results appear to be in very good accordance with the results obtained for the comprehensive Bailey [15] model. Signal intensities from this simplified three-energy-level model are ~30% higher than compared to the complete parameter set in the original model, which can be explained by the absence of competing traps in which electrons can be captured. Thus, the probability of a direct recombination with the L-centre is higher and consequently a higher signal intensity is observed. The curve shape after normalizing to the last value of the RF signal is in very good agreement with Fig. 6, justifying the application of the simplified model for further analyses.

In the following we used the simplified three-energy-level model. To better understand the dynamics of the charge flows in the system, a closer look at the numerical solutions is necessary. For this we investigated the concentrations of the deep trap and the two hole centres at the beginning of the RF step (see Table 3, step 10).

Fig. 9 shows the concentration of electrons in the deep trap and holes in the R-centre and the L-centre for the simplified model as a function of the preheat temperature after the preheat step and hence before the beginning of the RF simulation. The concentrations are normalized to the total amount of electrons in the system. The results of Fig. 9 strongly indicate that the model successfully describes the pre-dose activation process, which is believed to result from holes transferring from the R-centre into the L-centre during the heating of the sample in the temperature range 300–400 °C [16]. If the preheat temperature increases, the concentration of holes in the L-centre is increased, while the corresponding concentration of holes in the hole reservoir R

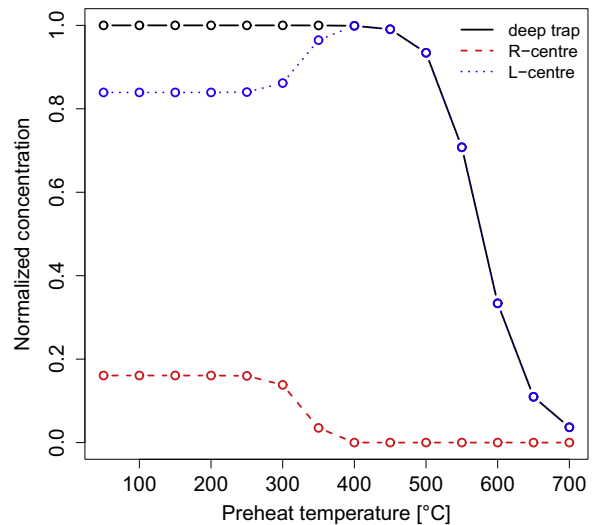


Fig. 9. The concentration of electrons in the deep trap and holes in the R-centre and the L-centre after the preheat step (step 9 in Table 3) for the simplified three-energy-level model. The values are normalized to the total amount of electrons.

decreases by the same total amount. The results of Fig. 9 also show that an activation temperature in the region of 300–400 °C is sufficiently high to transfer all holes from the hole reservoir R into the luminescence centre L. In contrast to the simulations by Pagonis et al. [35], Fig. 2b, the concentration of electrons does not remain constant during even higher temperatures, but decreases and so does the number of holes in the L-centre. This is possible because the temperatures are high enough to release electrons from the deep electron trap and charge neutrality forces the number of available holes to decrease; consequently the intensity of the luminescence signal decreases. This mechanism may explain the measured and simulated initial RF signal in Figs. 3 and 6 and it is capable of explaining why the decrease of the UV-RF signal is much weaker at temperatures above 550 °C.

Furthermore we investigated the behaviour for the initial UV-RF signal for different burial doses (see step 7 in Table 3). Fig. 10(a) shows the initial signal for different preheat temperatures from 50 °C to 500 °C and for different simulated burial doses in step 7 in the sample history of the quartz sample (see Table 3). The higher the simulated burial dose, the higher are the initial signals as well as the peak at 400 °C. A detailed view is provided by Fig. 10(b): The initial RF signal at

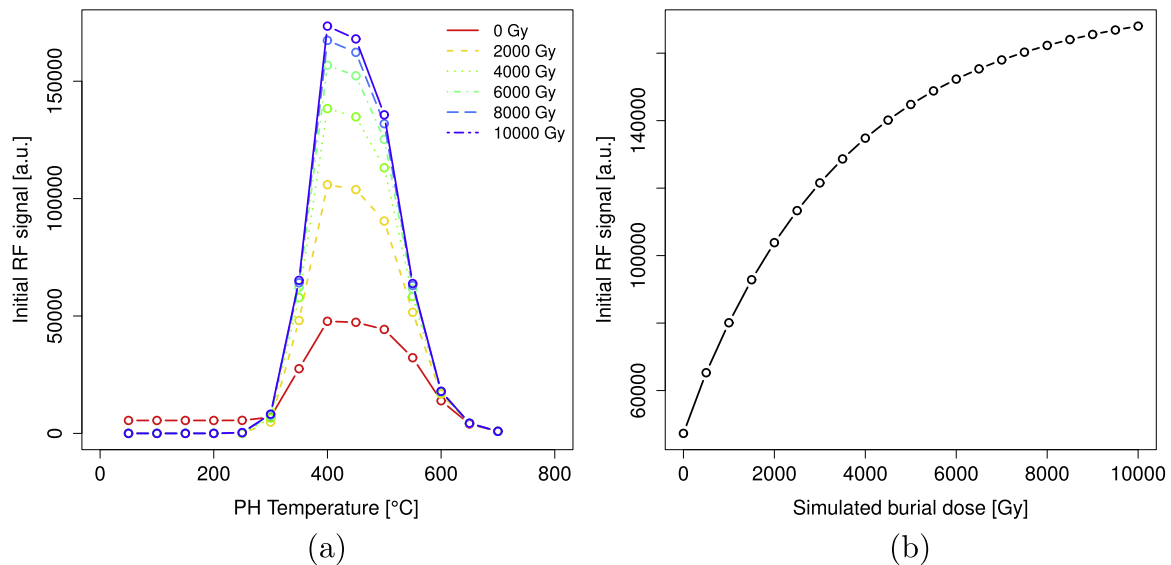


Fig. 10. Simulations for different burial doses for step 7 in the sample history (see step 7 in Table 3). (a) shows initial RF signals for different preheat temperatures and for 6 different burial doses. (b) is a detailed view on the initial RF signal at 450 °C. The initial signal was plotted against the simulated burial dose.

a preheat temperature of 450 °C is plotted against the simulated burial dose and an increasing dose-response curve can be extracted from the simulated data. Note that Fig. 10(a) only provides 6 different burial doses. Fig. 10(b) shows the numerical solution for burial doses from 0 Gy to 10,000 Gy using increments of 500 Gy.

In summary, the results of these simulations show that the initial signal of the quartz UV-RF depends on the burial dose. A multiple aliquot additive dose (MAAD) protocol with convenient preheat temperatures might be used for determining the burial dose. Marazuev et al. [21] first used this technique to determine the equivalent dose of quartz extracted from bricks in Chernobyl, but they used X-ray excitation. In their experiments, they focused on the difference between the initial signal and the signal after a certain time, the final kinetic equilibrium, and they used a preheat of 510 °C for 10 minutes. In contrast to our simulation findings, they observed a linearity in their dose-response curve for very low doses only. Nevertheless, our results indicate that with the UV-RF technique a determination of the equivalent dose in quartz is possible and needs to be (re-)investigated in a separate study.

5. Discussion

‘Modeling is important for the purpose of determining if suggested mechanisms can indeed produce the effects observed in the practice’ [37]. The presented model and the interpretation of the results show indeed the accordance of model predictions and experimental results. Nevertheless it is important to test the model to determine ‘what is possible with the model, and what is not possible’ [37]. We have run several tests with the parameter set presented in Table 2 (TL peak shift with different heating rates, thermal activation characteristics, dose-recovery tests, OSL behaviour; see supplementary material) and all investigated phenomena produced meaningful results.

Nevertheless, simulated results should always be handled with care, as they describe a phenomenological point of view. To use the dependency of the initial signal height on the burial dose as a dating method one important requirement is the zeroing of the luminescence signal. From Fig. 10 one can deduce that a non zero signal of the initial RF signal for a preheat temperature of 450 °C is obtained in simulations for a burial dose equal to zero. The growth of the initial RF signal with the burial dose is a result of the dose

dependence of the hole concentration in the luminescence centres (see Fig. 5). The concentration of this centre, however, is growing also before the zeroing event and optical bleaching is not sufficient to reduce it down to zero. Fig. 9 shows that this is in principle possible when heating a sample to very high temperatures. This is in accordance with the published literature for determining an equivalent dose with quartz UV-RF [21], because they used bricks to determine the radiation dose related to the Chernobyl accident [21]. When burning these bricks all electron traps and hole centres were emptied and the requirement of a complete zeroing the signal was fulfilled. Nevertheless, Marazuev et al. [21] also determined equivalent doses for natural quartzes but they also mentioned that this UV-RF approach will work for small doses only. Investigating this in detail is not part of this contribution.

As described in Schmidt et al. [9], RF offers new insights into the recombination centres, due to the fact that quartz RF signals are believed to correspond to the direct recombination of electrons from the conduction band. Schmidt et al. [9] argue that the RF technique provides information primarily on the recombination centres involved. Our results seem to confirm these ideas, since the increase of the initial RF signal appears to be a consequence of the movement of trapped holes from the reservoir centres to luminescence centres. In addition, our preheat experiments and simulations indicate that the deep traps play a fundamental role in the description of quartz RF signals. At high temperatures the deep traps get emptied and so does the concentration of holes in the luminescence centres (see Fig. 9).

It should also be noted that the rapid change in the initial RF height occurs after the transition from α - to β - quartz at a temperature of 573 °C (at normal pressure). Due to the fact that all RF measurements were performed at RT and the samples were cooled down from the preheat temperatures to RT in nitrogen atmosphere, a transition back from β - to α - quartz appears to be likely. This transition is not part of the simulations but in the simulations this behaviour is indicated by emptying the deep electron traps.

6. Conclusions

A systematic investigation of UV-RF signals on two quartz samples (BT586 and BT1196) after preheat temperatures ranging from 50 °C to 700 °C was presented. For both samples the behaviour was similar: for low temperatures no differences in the UV-

RF signal dynamics and in the initial signal height was observed. For preheat temperatures $>400\text{ }^{\circ}\text{C}$ a significant rise in the initial height was noticeable as well as a decreasing signal. The initial signal was increasing until a peak was reached at a preheat of $550\text{ }^{\circ}\text{C}$. From this temperature on, the signal intensity was decreasing rapidly. For sample BT586 a change in the signal dynamics was detected for very high preheat temperatures: the signal is not decreasing during the complete stimulation time but builds up until 3,000 s and then decreases. Note that BT1195 was completely bleached before the measurements and BT586 still carries its natural dose. Nevertheless, both samples show a very similar behaviour.

Another preheat experiment showed that the initial RF signals are rising, if repeated cycles of preheating to $500\text{ }^{\circ}\text{C}$ for 120 s and subsequent RF measurements were executed. These dynamics are similar to what is already known as the 'pre-dose' effect in quartz. This observation was similar for both samples.

In order to simulate these experimental results, a slightly modified Bailey [15] model was used successfully. The different initial signal intensities and dynamics of the UV-RF signal could be simulated with good accordance between numerical and experimental results.

In addition to the successful simulation of the experimental data, we used a simplified model with three energy levels to obtain further insights. A theoretical explanation of the observed decrease of the initial signal height for high preheat temperatures is given, because the deep electron traps are emptied and the available concentration of holes in the luminescence centre L is decreasing and so are the signal intensities. Simulations additionally showed that the height of the RF signal depends on the burial dose of the sample. Brik et al. [38] and Marazuev et al. [21] reported this and used this fact to determine the burial dose. However, further experiments and studies are needed to establish this pre-dose method.

Acknowledgements

Initial UV-RF measurements and preparation of the samples BT586 and BT1195 were carried out within the framework of the project "Radiofluorescence of quartz: Challenges towards a dating application" (DFG, 2013–2015, SCHM 3051/2-1 und FU 417/16-1 and DAAD-PPP USA, 2013–2014, Prof. Dr. Markus Fuchs, id: 56022859). JF is gratefully supported by the DFG (2015–2018, "Modelling quartz luminescence signal dynamics relevant for dating and dosimetry", SCHM 3051/4-1). SK was supported by the ANR (no. ANR-10-LABX-52). We also thank the two anonymous reviewers for their helpful suggestions.

Appendix A. Supplementary data

Supplementary data associated with this article can be found in the online version at <http://dx.doi.org/10.1016/j.jlumin.2017.02.039>.

References

- [1] R. Chen, S.W.S. McKeever, *Theory of Thermoluminescence and Related Phenomena*, World Scientific, Singapore, 1997.
- [2] V. Pagonis, G. Kitis, R. Chen, Applicability of the Zimmerman predose model in the thermoluminescence of predosed and annealed synthetic quartz samples, *Radiat. Meas.* 37 (2003) 267–274.
- [3] R. Chen, V. Pagonis, Modelling thermal activation characteristics of the sensitization of thermoluminescence in quartz, *J. Phys. D: Appl. Phys.* 37 (2004) 159.
- [4] A. Chruścińska, Modelling the thermal bleaching of OSL signal in the case of a competition between recombination centres, *Radiat. Meas.* 44 (2009) 329–337.
- [5] B. Subedi, G. Kitis, V. Pagonis, Simulation of the influence of thermal quenching on thermoluminescence glow-peaks, *physica status solidi (a)* 207, 2010, pp. 1216–1226.
- [6] R. Chen, V. Pagonis, *Thermally and Optically Stimulated Luminescence: A Simulation Approach*, John Wiley & Sons, Chichester, 2011.
- [7] V. Pagonis, M.L. Chithambo, R. Chen, A. Chruścińska, M. Fasoli, S.H. Li, M. Martini, K. Ramseyer, Thermal dependence of luminescence lifetimes and radioluminescence in quartz, *J. Lumin.* 145 (2014) 38–48.
- [8] E.O. Oniya, Dependence of heating rates of thermal activation on thermal activation characteristics of $110\text{ }^{\circ}\text{C}$ TL peak of quartz: a simulation approach, *Radiat. Phys. Chem.* 115 (2015) 171–178.
- [9] C. Schmidt, S. Kreutzer, R. DeWitt, M. Fuchs, Radiofluorescence of quartz: a review, *Quat. Geochronol.* 27 (2015) 66–77.
- [10] H. Fujita, T. Hashimoto, Influence of radioluminescence on optically stimulated luminescence from natural quartz grains, *Radioisotopes* 55 (2006) 117–123.
- [11] N. Shimizu, N. Mitamura, A. Takeuchi, T. Hashimoto, Dependence of radioluminescence on TL-properties in natural quartz, *Radiat. Meas.* 41 (2006) 831–835.
- [12] M. Martini, M. Fasoli, A. Galli, I. Villa, P. Guibert, Radioluminescence of synthetic quartz related to alkali ions, *J. Lumin.* 132 (2012) 1030–1036.
- [13] M. Martini, M. Fasoli, I. Villa, P. Guibert, Radioluminescence of synthetic and natural quartz, *Radiat. Meas.* 47 (2012) 846–850.
- [14] V. Pagonis, J.L. Lawless, R. Chen, C. Andersen, Radioluminescence in Al_2O_3 : C - analytical and numerical simulation results, *J. Phys. D: Appl. Phys.* 42 (2009) 175107.
- [15] R.M. Bailey, Towards a general kinetic model for optically and thermally stimulated luminescence of quartz, *Radiat. Meas.* 33 (2001) 17–45.
- [16] J. Zimmerman, The radiation-induced increase of the $100\text{ }^{\circ}\text{C}$ thermoluminescence sensitivity of fired quartz, *J. Phys. C: Solid State Phys.* 4 (1971) 3265–3276.
- [17] M. Fasoli, M. Martini, The composite nature of the thermoluminescence UV emission of quartz, *J. Lumin.* 173 (2016) 120–126.
- [18] G. Adamiec, Investigation of a numerical model of the pre-dose mechanism in quartz, *Radiat. Meas.* 39 (2005) 175–189.
- [19] V. Pagonis, H. Carty, Simulation of the experimental pre-dose technique for retrospective dosimetry in quartz, *Radiat. Prot. Dosim.* 109 (2004) 225–234.
- [20] N. Itoh, D. Stoneham, A.M. Stoneham, The predose effect in thermoluminescent dosimetry, *J. Phys.: Condens. Matter* 13 (2001) 2201.
- [21] Y.A. Marazuev, A.B. Brik, V.Y. Degoda, Radioluminescent dosimetry of α -quartz, *Radiat. Meas.* 24 (1995) 565–569.
- [22] T. Kolb, M. Fuchs, L. Zöller, Deciphering fluvial landscape evolution by luminescence dating of river terrace formation: a case study from Northern Bavaria, Germany, *Z. für Geomorphol. (Suppl. 60)* (2016) 29–48.
- [23] F. Preusser, D. Degering, M. Fuchs, A. Hilgers, A. Kadereit, N. Klases, M. Krbrtschek, D. Richter, J.Q.G. Spencer, Luminescence dating: basics, methods and applications, *Quat. Sci. J.* 57 (2008) 95–149.
- [24] D. Richter, A. Richter, K. Dornich, Lexsys - A new system for luminescence research, *Geochronometria* 40 (2013) 220–228.
- [25] D. Richter, R. Pintaske, K. Dornich, M. Krbrtschek, A novel beta source design for uniform irradiation in dosimetric applications, *Anc. TL* 30 (2012) 57–63.
- [26] R Development Core Team, R: A language and environment for statistical computing, Vienna, Austria, 2016.
- [27] S. Kreutzer, C. Schmidt, M.C. Fuchs, M. Dietze, M. Fischer, M. Fuchs, Introducing an R package for luminescence dating analysis, *Anc. TL* 30 (2012) 1–8.
- [28] S. Kreutzer, M. Dietze, C. Burrow, M. C. Fuchs, C. Schmidt, M. Fischer, J. Friedrich, N. Mercier, R. K. Smedley, J. Durcan, G. King, Luminescence: Comprehensive Luminescence Dating Data Analysis, CRAN version 0.6.2, 2016. Developer version on GitHub: (<https://github.com/R-Lum/Luminescence>).
- [29] J. Friedrich, S. Kreutzer, C. Schmidt, RLumModel: Modelling Ordinary Differential Equations Leading to Luminescence, CRAN version 0.1.2, 2016. Developer version on GitHub: (<https://github.com/R-Lum/RLumModel>).
- [30] J. Friedrich, S. Kreutzer, C. Schmidt, Solving ordinary differential equations to understand luminescence: RLumModel, an advanced research tool for simulating luminescence in quartz using R, *Quat. Geochronol.* 35 (2016) 88–100.
- [31] M. Martini, M. Fasoli, I. Villa, Defect studies in quartz: Composite nature of the blue and UV emissions, *Nucl. Instruments Methods Phys. Res. Sect. B: Beam Interact. Mater. Atoms* 327 (2014) 15–21.
- [32] M. Krbrtschek, T. Trautmann, A spectral radioluminescence study for dating and dosimetry, *Radiat. Meas.* 32 (2000) 853–857.
- [33] R.M. Bailey, B.W. Smith, E.J. Rhodes, Partial bleaching and the decay form characteristics of quartz OSL, *Radiat. Meas.* 27 (1997) 123–136.
- [34] J. Zimmerman, The radiation-induced increase of thermoluminescence sensitivity of the dosimetry phosphor LiF (TLD-100), *J. Phys. C: Solid State Phys.* 4 (1971) 3277–3291.
- [35] V. Pagonis, E. Balsamo, C. Barnold, K. Duling, S. McCole, Simulations of the predose technique for retrospective dosimetry and authenticity testing, *Radiat. Meas.* 43 (2008) 1343–1353.
- [36] V. Pagonis, G. Adamiec, C. Athanassas, R. Chen, A. Baker, M. Larsen, Z. Thompson, Simulations of thermally transferred OSL signals in quartz: accuracy and precision of the protocols for equivalent dose evaluation, *Nucl. Instruments Methods Phys. Res. Sect. B: Beam Interact. Mater. Atoms* 269 (2011) 1431–1443.
- [37] S.W.S. McKeever, R. Chen, Luminescence models, *Radiat. Meas.* 27 (1997) 625–661.
- [38] A.B. Brik, V.Y. Degoda, Y.A. Marazuev, X-ray luminescence dosimetry of irradiated quartz, *J. Appl. Spectrosc.* 60 (1994) 398–400.